DOR: 20.1001.1.27170314.2021.10.4.3.8

Research Paper

Mechanical Stability of RCSed and ECAPed Intramedullary 316L Stainless Steel Nails in the Treatment of Diaphyseal Bone Fractures

Abdolreza Rastitalab[1], Salar Khajehpour[1*], Ahmad Afsari[1], Shahin Heidari[2], Javad Dehghani[2]

[1]Department of Mechanical, Shiraz Branch, Islamic Azad University, Shiraz, Iran

[2]Bone and Joint Diseases Research Center, Shiraz University of Medical Sciences, Shiraz, Iran

[*]Email of Corresponding Author: khajehpour@iaushiraz.ac.ir

Received: August 25, 2021; Accepted: December 5, 2021

Abstract

Over the last several decades, implants have been used to treat fractures and promote healing. The most important reason for deformation and shortening of the bone during healing due to loading on the nails is a lack of strength of the intramedullary nail. Materials with very fine grain dimensions are considered for such purposes. Ultrafine-grained (UFG) materials have structural elements with very fine grain sizes. Several methods for producing UFG materials have been developed, one of which is the top-down approach, which refines coarse-grained metals via severe plastic deformation (SPD). The SPD technique has several advantages that set it apart from other methods of synthesizing. Two of the SPD methods used in this study were the repetitive corrugation and straightening (RCS) process and the equal channel angular pressing (ECAP) process on a 316L stainless steel rod. Mechanical tests were performed on the rods produced using these methods. Under loading, simulation results revealed that the bone implanted by the RCS rod has greater structural stiffness than the bone implanted by an ECAPed 316L stainless steel rod.

Keywords

Diaphyseal Bone Fractures, Intramedullary Nailing, Severe Plastic Deformation (SPD), Finite Elements Method

1. Introduction

Severe plastic deformation (SPD) produces ultrafine-grained (UFG) materials that are both dense (which is important for mechanical properties) and contamination-free (imperative for biomedical properties). High-pressure torsion (HPT), accumulative roll bonding (ARB), multipass coin-forging (MCF), and repetitive corrugation and straightening (RCS), continuously confined strip shearing (C2S2), and continuous strip shearing are all important strategies in this category (C2S2). Furthermore, SPD procedures are capable of producing bulk UFG materials in quantities suitable for orthopedic applications.

The intramedullary nail is one of several orthopedic implants that are commonly used to treat long bone fractures. In modern medicine, nail implantation techniques that cause the least amount of skin damage and require the least amount of time to reform the fractured bone are used. While using platinum and plaster to align fractured bones is not recommended due to several issues such as

remaining surgery wounds, limitation of the patient's activity due to the presence of additional support around the fracture site, and the possibility of breaking out the bone-inside screw and plaque [1],

One of the most significant advantages of the intramedullary nail is that it makes surgery easier, reduces surgery time, and reduces injury and rupture of the skin and tissue surrounding the bone. One of the fracture healing methods is intramedullary nailing, which is used to align the fractured bone. Furthermore, embedding and removing the intramedullary nail is too simple for a surgeon, and no external equipment is required; this is the reason for the lower infection rate in this method [2].

The most important reason for deformation and shortening of the bone during healing due to loading on the nail is a lack of strength of the intramedullary nail. In this regard, different diameters of stainless steel external intramedullary nails are manufactured. It is preferable to use a material with a high tensile strength because the lack of strength of the nail causes it to deviate and damage soft tissues around the bone [3].

There are numerous research projects today devoted to studying and improving the mechanical properties of metals. This is because of that this type of metal is widely used in medical industries due to its unique properties [4].

Many researchers have worked hard to develop high-strength stainless steel using the mechanical alloying process. With the advancement of the medical industries, it is becoming less necessary to improve the properties of stainless steel alloys, including high strength [5].

The main issue with the RCS method is the possibility of cracks forming due to tiny porosities. In general, factors such as impurities, which aid in increasing crystal structure strength, and structural defects such as grain boundaries and dislocations play a critical and determinative role in the creation of strength in stainless steel [6].

Polycrystalline materials with very fine grading of nanometers and/or hundreds of nanometers (less than a micron) have piqued the interest of many researchers over the last two decades due to their unique mechanical and physical properties. Based on the scientific literature presented, a suitable method to improve the mechanical properties of high tensile strength stainless steel must be presented and developed. The mechanical and physical properties of crystalline materials are influenced by a variety of factors, one of which is medium grain size. In general, the Hall-Petch relation states that decreasing the grain size increases the material's strength [7]. The Hall-Petch Eq. (1) is described as follows:

$$\sigma_x = \sigma_y + \mathrm{k}d^2 \qquad (1)$$

In the above Eq. (1), σ_x is the friction stress generated inside the channel, σ_y is the applied stress that is imposed on the workpiece by a plunger, *d* is the grain size and *k* is the constant of proportionality which is known as the constant of yielding.

The strain occurring on the workpiece while performing ECAP is measured by Eq. (2) which helps in calculating equivalent strain which occurs in the workpiece when it is subjected to a certain value of the number of passes. The equation for the calculation of equivalent strain is described as follows:

$$\varepsilon \mathrm{N} - \mathrm{N}\frac{N}{\sqrt{3}}\left[2\cot\left(E_{02}+\frac{\emptyset}{2}\right)+\emptyset csc\left(E_{02}+\frac{\emptyset}{2}\right)\right] \qquad (2)$$

Where ε is the equivalent strain, which is observed while ECAP, N is the number of passes, ϕ is the channel angle of the die and W is the corner angle of the channel.

SPD is one of the new methods for producing nanometer-grain materials. The size of grains in this method is reduced to the nanoscale by applying severe strains to the sample, resulting in a dramatic improvement in the mechanical properties of metal. Because material dimension changes can impede the applied strain, most SPD methods are designed so that the sample dimensions do not change during the process. The production process of UFG materials was investigated in this study using SPD. These studies discovered a link between very grain refinement, a very high volume fraction of grain boundaries, and polycrystalline exclusive deformation behavior under superplastic conditions [8].

Hussain et al. [9] reviewed different processes of Severe Plastic Deformation and its effect on Titanium and its application. They reviewed the mechanical properties of Titanium being subjected to different kinds of load while being processed through different SPD processes. They eventually found that the nano-structured titanium has a much-refined grain structure and its scope of application is also very wide [9].

Lin and Wang [10] have reviewed the biomedical titanium alloys and the effects
of SPD processes particularly High-Pressure Torsion (HPT), Accumulative Roll Bonding (ARB), and Friction Stir Processing. In their review, they concluded that by the use of Grain refinement techniques such as SPD, the mechanical and biological properties of the titanium alloys can be enhanced and this could further lead to the wide application of titanium alloys under different conditions.

Niinomi [11] studied the various alloying elements which are used to synthesize biomedical titanium alloys. Elements like Nb, Ta, and Zr are used as alloying elements with titanium depending upon the application. He conducted various tests on the titanium alloy specimen and concluded that the biomedical applications of titanium are immense and the properties of these alloys could be enhanced by the grain refinement techniques such as SPD which enhances the mechanical properties and biocompatibility of these alloys.

Miroslav et al. [12] studied the deformation behavior of the titanium alloys under the ECAP process. They prepared the titanium from commercially pure titanium by extrusion. SEM and TEM images of the sample before and after ECAP were also analyzed to study the grain refinement. The mechanical properties such as tensile properties were observed to be increased up to 960 MPa upon grain refinement by the ECAP process. They concluded that ECAP is one of the best grain refinement processes to enhance the mechanical and biomedical properties of titanium alloys.

D. P.de Oliveira [13] had taken a sample of Ti-6Al-7Nb alloy and performed SPD processes on it to observe the changes in the surface properties and mechanical properties of the alloy. It was observed that after refining the grains of the titanium alloy, the surface properties enhanced along with the mechanical properties of the alloy.

To create intramedullary nails, two methods of SPD were used in this study. RSC and Equal Channel Angular Pressing (ECAP) are two of them [14].

The workpiece bends and flattens repeatedly during the RCS process, with no discernible change in the cross-sectional area. The RCS process's main cycle consists of two steps. As a result, a large plastic strain is applied to the material, resulting in the formation of a very fine structure [15].

This method is also capable of producing bulk nanostructure materials without pollution or porosity on an industrial scale. By pressing a material through a special die, ECAP imparts a plastic strain without causing a change in the cross-section dimensions of the pressed sample. The steel with modified properties has an intriguing combination of flexibility and tensile strength. To summarize, these steels can be an excellent substitute for intramedullary nails in terms of preventing bone deformation and damage. The steel industry continues to produce modern high-quality steels known as advanced steels. This is due to increased tensile strength, better plasticity, and more reasonable toughness, all of which are obtained by improving microstructure [16].

Transformation induced Plasticity Steel (TRIP) results from the transformation of unstable retained austenite to martensite during deformation at room temperature. TRIP steels have this property, which allows them to be both plastic and strong [17, 18].

In this study, the RSC and ECAP processes were used to induce SPD in stainless steel rods. As a result of the RSC process and ECAP, the compressive stiffness of the nails used to implant in a fractured bone increases, allowing the implanted bone to withstand greater applying forces.

2- Materials and methods

2.1 Material properties

316L stainless steel was used to repair the broken bone because of its reasonable combination of mechanical properties, corrosion resistance, and reasonableness in comparison to other materials. This metal is a stainless alloy composed of austenitic chromium, nickel, and molybdenum that resists corrosion well. This steel is created through modifications such as the addition of chromium and the reduction of carbon. Low carbon content reduces chromium carbide sedimentation, which has a direct impact on grain boundary corrosion [19].

Austenite is a body-centered cubic (BCC) iron phase that is stable in iron without alloying elements at temperatures ranging from 910°C to 1400°C. The lack of magnetic properties indicates that these alloys are nonmagnetic due to their austenitic matrix and structure. Austenite can be made stable at room temperature by adding austenitic elements such as nickel. This phase change primarily changes the mechanical properties of the alloy, including its plasticity. Because of the austenite phase, these alloys are non-magnetic when tempered, but a slight magnetic characteristic may be produced as a result of phase change in the cold work state [20].

The chemical composition of 316L stainless steel was measured using spark emission spectroscopy (SES) and compared to the ASTM A240 standard, as shown in Tables 1 and 2. (Tables 1 and 2)

Table 1. The mechanical properties of 316L stainless steel

Vickers 2 (hardness)	Elongation 2 in %50 mm (%)	Yield stress 1 (MPa)	Ultimate tensile strength 1 (MPa)
155	60	205	515

Table 2. The Chemical compound of 316L used for WT %

Fe	Si	P	N	C	S	Mn	Mo	Ni	Cr	Element
base	0.75	0.045	0.1	0.03	0.03	2	2.5	12	17	Weight percent
base	0.75	0.045	0.1	0.03	0.03	2	3-2	14-10	18-16	Weight percent [15]

2.2 Intramedullary nails made by RSC process

The RCS cycle has two steps: corrugation and straightening/rolling. The first step is to corrugate the workpiece, which is done with a recently designed and built persistent RCS facility, as shown in Figure 1(a). The second step is to straighten the workpiece by rolling it through a standard rolling process. Figure 1(b). illustrates the bar which was created by the RSC process [21, 22].

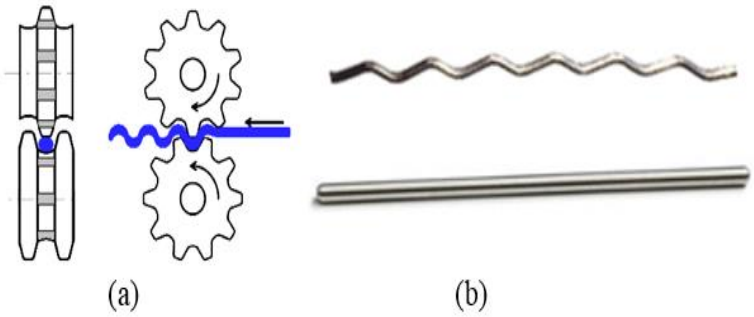

Figure 1. a) Schematic illustration of the RCS process b) The nail produced by the RCS process

2.3 Intramedullary nails created using the ECAP process

A well-lubricated sample of material is squeezed by a plunger in a special die to pass it through two crossing channels meeting at a diagonal point known as the die channel point, and plastic strain is imposed by simple shear at the intersection of the channels (Figure 2). A shear strain is introduced as the billet passes through the point of intersection of the two channels. Unlike conventional deformation processes such as rolling, fashioning, drawing, and so on, the pressings in this method can be repeated as long as the billet dimensions remain constant, allowing for exceptionally high strains with homogeneous equiaxed grains [23, 24].

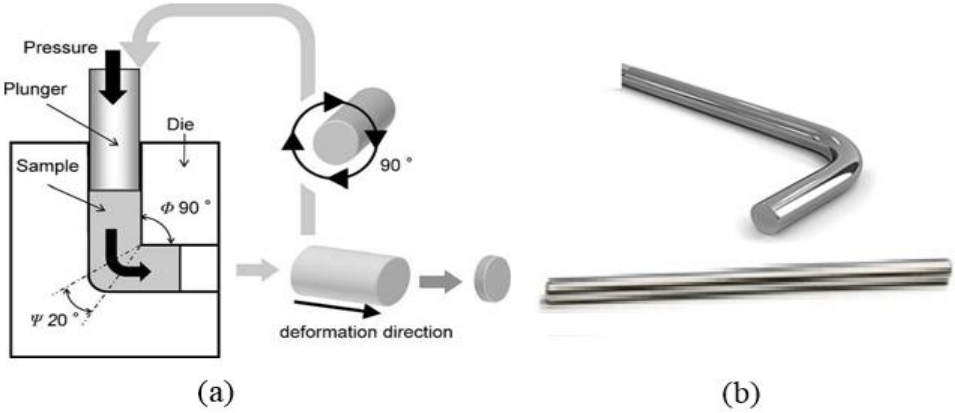

Figure 2. a) Schematic illustration of the ECAP process b) The nail produced by the ECAP process

2.4 Microstructural Analysis

An IEI- IMM420 optical microscope was used to examine the cross-sections microstructure of 316L stainless steel processed via the RCS and ECAP. Furthermore, an Explorer X-Ray Diffraction (XRD) made by GNR was used to evaluate the chemical composition, morphology, and grain size of the samples. All samples were prepared for the tension test based on the ASTM E8/E8M-16a standard

and were cut to the desired dimensions using a wire-cut machine. For all samples and the base metal, the tension test was performed at a constant speed of 1 mm/min at room temperature [25, 26].

2.5 The pre-bent elastic rod implanted in a bone with a middle fracture is simulated

The C-shaped elastic model was used in this study for the implant rod in the bone with a middle fracture. To make this nail, the initial and produced samples were cut to a length of 300 mm in the eighth pass on a wire-cut machine. This rod has a diameter of 3 mm; after cutting the samples and machining the operation, two sides of the rod were ground for finishing.

Two 3-mm elastic nails with a pre-flexural radius equal to the canal diameter were inserted into the fractured bone. The nails were inserted into the bone canal from both ends. For this example, the loading was applied sequentially using the material property testing system. The loading rate was set to one millimeter per minute (Figure 3).

To investigate the stability of the fractured bone, two elastic rods were prepared: one made of 316L stainless steel by the RSC process and one made of ECAP stainless steel by the ECAP process. Two prepared flexible rods with a 3 mm diameter and a length of 300 mm were embedded in the pre-bent form through two 4 mm holes slightly lower than the bone's growth plane. Indeed, pre-bending is a common method used by orthopedic surgeons to increase bone strength by increasing surface contact between the rod and the bone [27]. This is done without any scientific argumentation, although the exact value of the pre-bending radius and the location of the rod's bending are unknown. This problem, however, can be solved by presenting a logical solution [28-29]. According to the fracture of the bone and the need for additional protection, the loading is less than that of a regular walking process; this was taken into account in our investigations [30].

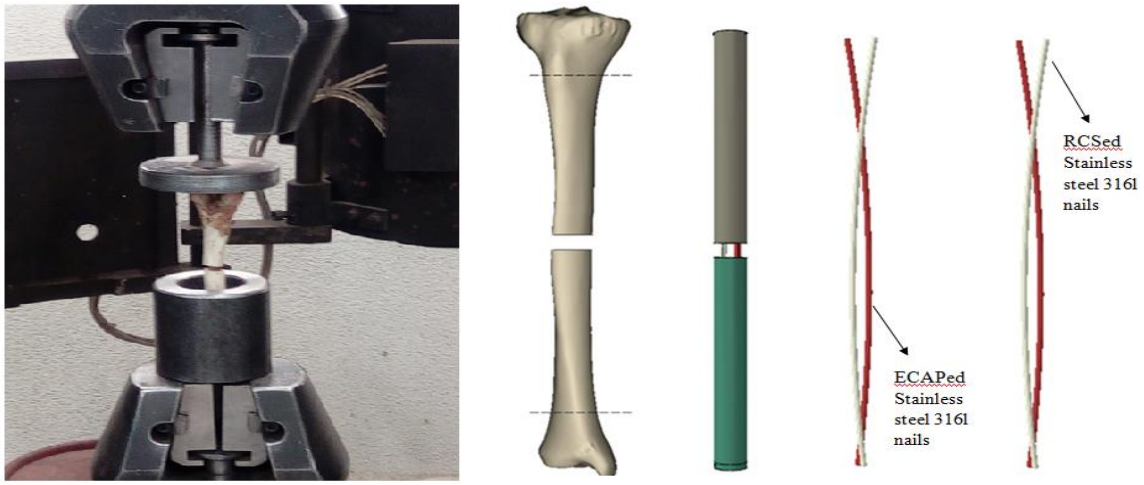

Figure 3. The implant simulation of elastic rods made of 316L (RCSed) and ECAPed stainless steel in the bone with middle fracture

3. Results and discussion

3.1 Microstructure examination

Figure 4 shows different grain size values obtained from the Williamson-Hall method for various steps of the RSC process and ECAP process. The grain size of the tested samples was determined using X-ray diffraction analysis. To analyze the X-ray diffraction results, the peaks associated with

each plane were first separated, and the index of planes was identified. The peaks corresponding to each of the differentiation planes were then determined using ORIGIN software, with the intensity of the reflected beam in terms of two. The analysis revealed that the grain size in the RCSed sample is much smaller than in the ECAPed sample, which explains why the RCSed samples are more stable.

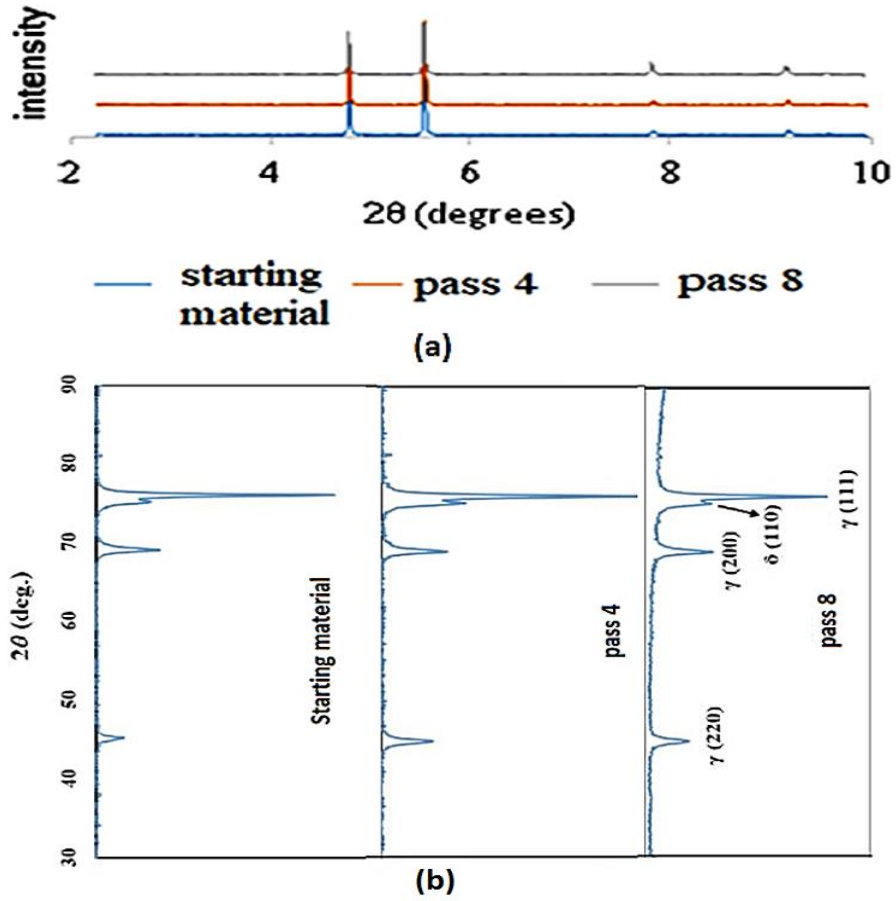

Figure 4. a) X-ray diffraction patterns were obtained from a) the RCSed sample b) the ECAPed sample

Table 3 displays the results of the WH method for estimating specimen dislocation density. As can be seen, the dislocation density of the alloy increases as the RCS pass number increases in comparison to the ECAP pass number. Furthermore, the main increase in dislocation density occurs after the imposition of the first RCS pass, whereas subsequent ECAP passes have less of an effect on the increase in dislocation density.

Table 3. The dislocation density of different specimens evaluated by the WH method (The unit of the values is $1/m^2$)

Pass No.	Dislocation density ECAP	Dislocation density RCS
0	4.25×10^{14}	4.25×10^{14}
2	2.21×10^{14}	7.21×10^{14}
4	4.08×10^{14}	9.11×10^{14}
6	5.23×10^{14}	11.01×10^{14}
8	6.25×10^{14}	1.01×10^{14}

3.2 Mechanical properties

Figure 5 depicts mechanical properties data extracted from tensile test results. The results showed that increasing the number of cycles increased the values of strength (UTS) in RCSed samples much more than in ECAPed samples.

The results clearly show that increasing the number of RCS cycles gradually increases hardness, which is consistent with the results of the microstructure development during the RCS process.

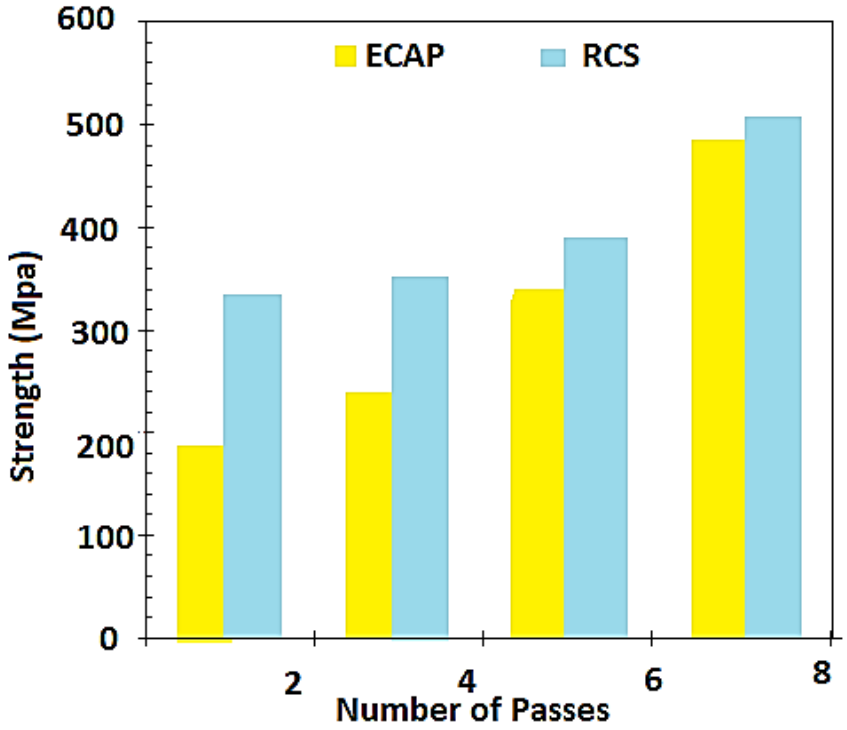

Figure 5. Strength variations of 316L stainless steel for various RCS and ECAP cycles

As shown in Table 4, the RCS process increased mechanical properties when compared to the ECAP process. A high Hardness Vickers value indicates that the material's workability improves during RCS cycles. The reason for this is due to finer grains and higher dislocation density in the RCSR process, as demonstrated by EBSD and XRD results when compared to the ECAP process.

Table 4. The mechanical properties of the RCSed and ECAPed implanted elastic rods

ECAPed nail	RCSed nail	Mechanical property
468	565	Hardness Vickers
856	913	Ultimate stress (MPa)
453	596	Yield stress(MPa)
624	780	Young's Modulus (GPa)
0.25	0.12	Poisson's ratio

3.3 Tensile strength of intramedullary nails

Figure 6 compares the compression stiffness of samples produced by the RSC method and samples produced by the ECAP method. As seen, the compression stiffness of the RCS process is greater than

that of the ECAP process. This is due to the RCS process producing nails with higher yield and compressive strengths based on grain size.

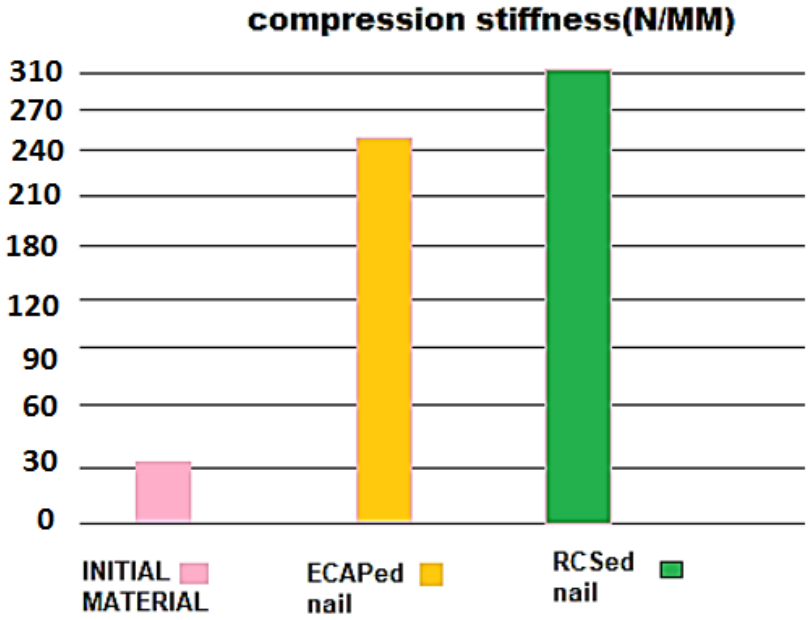

Figure 6. Compression stiffness variations of 316L stainless steel for RCSed and ECAPed nail

3.4 Deformation of the gap

The simulation results showed that the gap deformation under axial loading in fractured bone implanted with C-shaped nails made of RCSed 316L stainless steel rod is less than the gap deformation in the ECAPed 316L stainless steel rod. Figure 7 depicted the experimental compression test; the loading with the gap completely closed was labeled "ultimate load," and the relationship between force and displacement at the initial linear stage was labeled "linear stiffness" for comparison. As demonstrated, fractured bone implanted with RCSed nails can withstand more compression force than bone implanted with ECAPed nails.

If an axial load (F) is applied along the long axis of the implanted bone of length (L), the resulting deformation ΔL (shortening or elongation) is given by the equation (3):

$$\Delta L = \frac{FL}{E.A} \qquad (3)$$

Where E = Young's modulus and A = mean cross-sectional area. The product E.A is referred to as axial rigidity of the implanted bone and is measured in Newtons (N). As per equation (4) it can be noted that:

$$E.A = \frac{FL}{\Delta L} \qquad (4)$$

Axial linear stiffness (K) of the implanted bone is defined as the force required to produce a unit deflection. It is measured in N / mm and is given by the equation (5):

$$\mathrm{K} = \frac{\mathrm{E.A}}{\mathrm{L}} \quad (\text{Substituting} \quad \mathrm{E.A} = \frac{\mathrm{FL}}{\Delta \mathrm{L}}) \qquad \mathrm{K} = \frac{\mathrm{F}}{\Delta \mathrm{L}} \qquad (5)$$

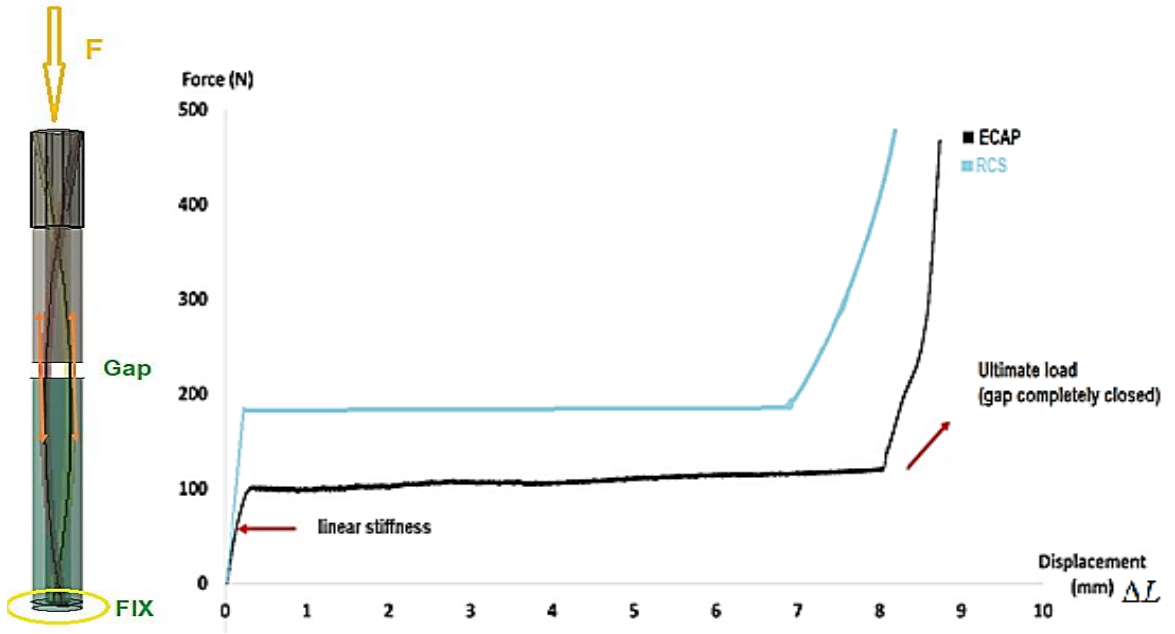

Figure 7. Gap deformation (ΔL)(mm) under compression in the implanted bone by the RCSed and ECAPed nails

4. Conclusion

The characteristics of intramedullary nails produced by the RCS and ECAP processes were studied in this study. The compression stiffness of the implanted 316L stainless steel rods in the fractured bone was investigated. Furthermore, the biomechanical behavior of ECAPed and RCSed rods was compared using an experimental test on the fractured bone. According to the scientific findings, the mechanical properties of the 316L stainless steel rod made by the RCS process were significantly improved over the mechanical properties of the ECAP nails. The simulation results revealed that the structural hardness of the 316L stainless steel rod produced by the RSC process in the eighth pass is greater under axial loading than the structural hardness of the 316L stainless steel rod produced by the ECAP process. When compared to an ECAPed 316L stainless steel rod, the deformation under pressure in the 316L stainless steel rod produced by the RSC process in the eighth pass is lower; this was one of the emphasis points in changing the properties of the rod. Because of the higher dislocation density available in the 316L stainless steel rod produced by the RSC process, the mechanical properties of the 316L stainless steel rod produced by the RSC process were higher than those of an ECAPed 316L stainless steel rod. There were some limitations to this study. To simplify the analysis, soft tissue forces such as muscles and ligaments were ignored, and only partial forces of body weight were taken into account. Muscular force and ligament-induced stress were not taken into account. Clinically, a fractured bone should be protected immediately after surgery. Furthermore, even after the bone has been welded with a rod, light weight-bearing is usually advised. As a result, the loading condition chosen for this study was only the evaluation of fractured bone strength, which does not include strength after callus (bone inner membrane) formation.

5. References

[1] Srivastava, A.K., Mehlman, C.T., Wall, E.J. and Do, T.T. 2008. Elastic stable intramedullary nailing of tibial shaft fractures in children. Journal of Pediatric Orthopaedics. 28(2): 152-158.

[2] Rastitalab, A., Khajepour, S., Dehghani, J., Afsari, A. and Heidari, S. 2021. Evaluating the Stability of the Fractured Bone Implanted with Titanium Elastic Nails in C and S Configurations. Journal of Hunan University Natural Sciences. 48(9): 349-357.

[3] Perren, Stephan M., 1989. The biomechanics and biology of internal fixation using plates and nails. Orthopedics; Thorofare. 12(1): 21-34.

[4] Chen, X.H., Lu, J., Lu, L. and Lu, K. 2005. Tensile properties of a nanocrystalline 316L austenitic stainless steel. Scripta materialia. 52(10): 1039-1044.

[5] Vilotić, M., Dačević, N., Milutinović, M., Movrin, D. and Siđanin, L. 2020. New severe plastic deformation method for 316l medical grade steel processing new SPD method for 316L steel processing. Acta Technica Corviniensis-Bulletin of Engineering. 13(1): 13-16.

[6] Wang, D., Song, C., Yang, Y. and Bai, Y. 2016. Investigation of crystal growth mechanism during selective laser melting and mechanical property characterization of 316L stainless steel parts. Materials & Design. 100: 291-299.

[7] Tahavvor, A.R., Zarrinchang, P. and Heidari, S. 2015. Numerical simulation of turbulent airflow in a human upper respiratory system. Modares Mechanical Engineering. 14(15): 267-272.

[8] Heidari, S. and Afsari, A. 2021. Study of Mechanical Properties of 7075 Aluminum Alloy Due to Particle Size Reduction due to Constrained Groove Pressing CGP Process. Journal of Modern Processes in Manufacturing and Production. 10(1): 5-18.

[9] Husaain, Z., Ahmed, A., Irfan, O.M. and Al-Mufadi F. 2017. Severe plastic deformation and its application on processing titanium: a review. International Journal of Engineering and Technology. 9(6): 426-431.

[10] Zhengjie, L., Liqiang, W., Kelvin, W.K.Y. and Jining, Q. 2013. The ultrafine-grained titanium and biomedical titanium alloys processed by severe plastic deformation (SPD). SOJ Materials Science & Engineering. 1(1): 1-5.

[11] Niinomi, M. 2008. Biologically and mechanically biocompatible titanium alloys.Materials transactions. 49(10): 2170-2178.

[12] Greger, M., Kander, L., Snášel, V. and Černý, M. 2011. Microstructure evolution of pure titanium during ECAP. Materials and Design. 18: 97-104.

[13] de Oliveira, D.P., Toniato, T.V., Ricci, R., Marciano, F.R., Prokofiev, E., Valiev, R.Z., Lobo, A.O. and Júnior, A.M.J. 2019. Biological response of chemically treated surface of the ultrafine-grained Ti–6Al–7Nb alloy for biomedical applications. International journal of nanomedicine. 14: 1725-1730.

[14] Heidari, S., Afsari, A. and Ranaei, M.A. 2020. Increasing Wear Resistance of Copper Electrode in Electrical Discharge Machining by Using Ultra-Fine-Grained Structure. Transactions of the Indian Institute of Metals. 73(11): 2901-2910.

[15] Mirsepasi, A., Nili-Ahmadabadi, M., Habibi-Parsa, M., Ghasemi-Nanesa, H. and Dizaji, A.F. 2012. Microstructure and mechanical behavior of martensitic steel severely deformed by the novel technique of repetitive corrugation and straightening by rolling. Materials Science and Engineering. A. 551: 32-39.

[16] El-Tahawy, M., Pereira, P.H.R., Huang, Y., Park, H., Choe, H., Langdon, T.G. and Gubicza, J. 2018. Exceptionally high strength and good ductility in an ultrafine-grained 316L steel processed by severe plastic deformation and subsequent annealing. Materials Letters. 214: 240-242.

[17] Heidari, S., Bakhshan, Y., Khorshidi Mal Ahmadi, J. and Afsari, A. 2019. Investigating the Behavior of Aluminum 7075 under the Process of CGP as the Fin of Space Structures. Modares Mechanical Engineering. 19(5): 1187-1197.

[18] Sudhakar, K.V. 2005. Metallurgical investigation of a failure in 316L stainless steel orthopaedic implant. Engineering Failure Analysis. 12(2): 249-256.

[19] Liu, G., Li, J., Zhang, S., Wang, J. and Meng, Q. 2016. Dilatometric study on the recrystallization and austenization behavior of cold-rolled steel with different heating rates. Journal of Alloys and Compounds. 666: 309-316.

[20] Steel, S., ASTM A 167 or ASTM A 240/A 240M. Type [304][316][304 or Type 316]. 2011. Atlas Steels Technical Department. Stainless Steel Grade Datasheets: 1-57.

[21] Pandey, S.C., Joseph, M.A., Pradeep, M.S., Raghavendra, K., Ranganath, V.R., Venkateswarlu, K. and Langdon, T.G. 2012. A theoretical and experimental evaluation of repetitive corrugation and straightening Application to Al–Cu and Al–Cu–Sc alloys. Materials Science and Engineering. A. 534: 282-287.

[22] Tahavvor, A.R., Heidari, S. and Zarrinchang, P. 2016. Modeling of the height control system using artificial neural networks. Journal of Agricultural Machinery. 6(2): 350-361.

[23] Yanushkevich, Z., Dobatkin, S.V., Belyakov, A. and Kaibyshev, R. 2017. Hall-Petch relationship for austenitic stainless steels processed by large strain warm rolling. Acta Materialia. 136: 39-48.

[24] Wang, Y., Yue, W., She, D., Fu, Z., Huang, H. and Liu, J. 2014. Effects of surface nanocrystallization on tribological properties of 316L stainless steel under MoDTC/ZDDP lubrications. Tribology International. 79: 42-51.

[25] Schomer, J.J. and Dapino, M.J. 2017. High temperature characterization of fiber bragg grating sensors embedded into metallic structures through ultrasonic additive manufacturing In Smart Materials, Adaptive Structures and Intelligent Systems. American Society of Mechanical Engineers. 58264: V002-5A003.

[26] Magno, I.A.B., Souza, F.V.A.D., Barros, A.D.S., Costa, M.O., Nascimento, J.M., Costa, T. and Rocha, O. 2017. Effect of the T6 heat treatment on microhardness of a directionally solidified aluminum-based 319 alloy. Materials Research. 20: 662-666.

[27] Tahavvor, Ali Reza, Pouya Zarrinchang, Iranagh Soroush Abadi, and Shahin Heidari.2017. Numerical simulation of realistic human lumbar spine model under compressive force, axial rotation and lateral bending loads. Modares Mechanical Engineering .16 (11): 54-60.

[28] Goodwin, R.C., Gaynor, T., Mahar, A., Oka, R. and Lalonde, F.D. 2005. Intramedullary flexible nail fixation of unstable pediatric tibial diaphyseal fractures. Journal of Pediatric Orthopaedics. 25(5): 570-576.

[29] Ligier, J.N., Metaizeau, J.P., Prevot, J. and Lascombes, P. 1985. Elastic stable intramedullary pinning of long bone shaft fractures in children. Zeitschrift für Kinderchirurgie. 40(04): 209-212.

[30] Anderson, R.T., Pacaccio, D.J., Yakacki, C.M. and Carpenter, R.D. 2016. Finite element analysis of a pseudoelastic compression-generating intramedullary ankle arthrodesis nail. Journal of the mechanical behavior of biomedical materials. 62: 83-92.